Electrochemical and Oxidation Behaviour of SMAT Alloy 800 SG Tubing Specimens

M.G. Faichuk[1,2], S. Ramamurthy[1], J.J. Nöel[2] and D.W. Shoesmith[1,2]
[1]Surface Science Western and [2]Department of Chemistry
The University of Western Ontario, London, Ontario, Canada N6G 0J3

Abstract

Stress Corrosion Cracking (SCC) of Alloy 600 (A600) steam generator (SG) tubing is the single most important reason that nuclear SGs are being replaced in Canada with Alloy 800 (A800). Though the incidence of cracking in A800 during SG operation has been minor, laboratory simulations and recent operational experience suggest that, under some operating conditions, SCC can still occur at locations that have sustained mechanical damage (such as fretting, dings and dent marks) during manufacturing and/or operation. Thus, there is an incentive to modify SG tubing properties to improve their corrosion resistance.

It is generally accepted that SCC of SG tubing is intergranular, i.e. corrosion prior to and/or during crack initiation and during crack growth occur most commonly at regions below the outer tube surface along some grain boundary paths. Consequently, surface modification using surface mechanical attrition treatment (SMAT) is being investigated. SMAT is a variation of shot peening and employs an ultrasonic vibration to bombard the specimen with small metallic, ceramic or glass balls. Compared to conventional shot peening, much larger diameter balls are used in the SMAT. These balls are spherical with a smooth surface and the velocity employed in the SMAT process is much lower (1–20 m/s) than the 100 m/s used in conventional shot peening.

The major objective of this project is to determine the effect of SMAT on the electrochemical and oxidation behaviour of A800 tubing in deaerated 0.1 M $Na_2S_2O_3$ solution, chosen because A600 is susceptible to SCC in this medium [1].

Preliminary optical and SEM/EDX analyses on SMAT samples did not detect any grain refinement in the outer surface layers and the tube microstructure did not change. However, Knoop microhardness measurements indicated a greater hardness of the SMAT surface compared to the untreated sample. The peak hardness occurred within 50 μm of the outer surface. Also, samples treated for longer times exhibited greater surface hardness compared to the shorter treatment times.

Anodic polarization measurements indicated the SMAT samples exhibited a corrosion potential ~ 100 mV more negative than those for the untreated sample. This also extended the passive region by about 100 mV for the SMAT samples. Electrochemical impedance spectroscopy (EIS) indicated a two-layer oxide structure with a compact barrier layer and an outer oxide. Equivalent circuit modeling was used to determine the oxide layer resistances as a function of applied potential, Figure 1. Two of the three SMAT samples displayed resistances higher than for the untreated A800, but this was due to the shift in corrosion potential, resulting in earlier passivation. As the potential was increased through the passive region, the effects of SMAT were shown to be detrimental, the resistance of the barrier layer for all of the treated samples being lower than for the untreated A800, indicating SMAT may not improving the corrosion resistance of A800 tubing.

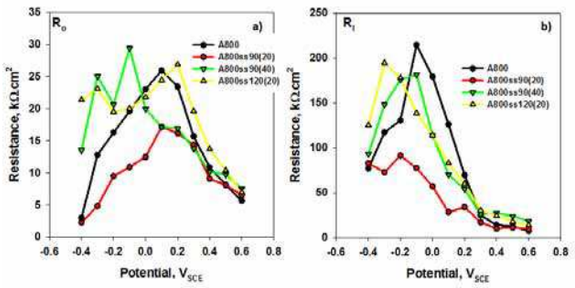

Figure 1. Figure 7. Resistance values for the outer (left) and the barrier oxide (right) layers as a function of applied potential

X-ray photoelectron spectroscopy (XPS) and scanning Auger microscopy (SAM) were employed to determine the influence of SMAT on the composition of the oxide layer formed at different applied potentials. High-resolution spectra were recorded for Ni 2p, Cr 2p and Fe 2p peaks. The results for the Cr 2p high-resolution spectra, Figure 2, indicate that the SMAT samples have a large $Cr(OH)_3$ component in the initial stages of the passive region. These results have been used to create a stoichiometric model of the oxide structure on A800 surface and the changes induced by SMAT have been identified.

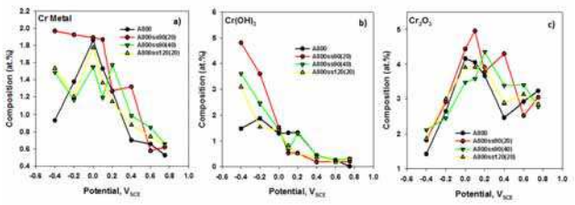

Figure 2. Changes in the a) Cr metal, b) $Cr(OH)_3$ and c) Cr_2O_3 components of the high resolution XPS Cr $2p_{3/2}$ spectra.

Reference

[1] W.-T. Tsai, C.-S. Chang, J.-T. Lee, Corrosion 50 (1994) 98–106